NO decomposition and reduction on Pt/Al$_2$O$_3$ powder and monolith catalysts using the TAP reactor[☆]

Ashok Kumar, Vinay Medhekar[1], Michael P. Harold [*], Vemuri Balakotaiah [*]

Department of Chemical and Biomolecular Engineering, University of Houston, Houston, TX 77204-4004, United States

ABSTRACT

A systematic study over Pt/Al$_2$O$_3$ powder and monolith catalysts is carried out using temporal analysis of products (TAP) to elucidate the transient kinetics of NO decomposition and NO reduction with H$_2$. NO pulsing and NO–H$_2$ pump-probe experiments demonstrate the effect of catalyst temperature, NO–H$_2$ pulse delay time and H$_2$/NO ratio on N$_2$, N$_2$O and NH$_3$ selectivity. At lower temperature (150 °C) decomposition of NO is negligible in the absence of H$_2$, indicating that N–O bond scission is rate limiting. At higher temperature NO decomposition occurs readily on reduced Pt but the rate is inhibited by surface oxygen as reaction occurs. The reduction of NO by a limiting amount of H$_2$ at lower temperature indicates the reaction of surface NO with H adatoms to form N adatoms, which react with adsorbed NO to form N$_2$O or recombine to form N$_2$. In excess H$_2$, higher temperatures and longer delay times favor the production of N$_2$. The longer delay enables NO decomposition on reduced Pt with the role of H$_2$ being a scavenger of surface oxygen. Lower temperatures and shorter delay times are favorable for ammonia production. The sensitive dependence on delay time indicates that the fate of adsorbed NO depends on the concentration of vacant sites for NO bond scission, necessary for N$_2$ formation, and of surface hydrogen, necessary for hydrogenation to ammonia. A mechanistic-based microkinetic model is proposed that accounts for the experimental observations. The TAP experiments with the monolith catalyst show an improved signal due to the reduction of transport restrictions caused by the powder. The improved signal holds promise for quantitative TAP studies for kinetic parameters estimation and model discrimination.

© 2009 Elsevier B.V. All rights reserved.

1. Introduction

NO$_X$ storage and reduction (NSR) is a promising technology for meeting upcoming stringent regulations for lean burn engines [1–3]. The technology consists of treating excess NO$_X$ which is not converted in the diesel oxidation catalyst (DOC) zone into benign products such as N$_2$, CO$_2$, and H$_2$O. As of today, there is no current single-stage catalyst technology that can reduce NO$_X$ in the presence of excess oxygen without adding a reductant. Both NSR and ammonia-based selective catalytic reduction (SCR) are viable solutions with their unique advantages and disadvantages [4,5]. SCR appears best-suited for heavy-duty applications while NSR is a viable process for light-duty lean burn and diesel vehicles. Our efforts are focused on understanding the elementary processes occurring on the catalyst surface during NSR, which will help in the catalyst design and optimization.

NSR consists of two stages of operation. The first stage involves the storage of NO$_X$ on alkaline earth or alkali metal mediated by precious metal to convert NO to NO$_2$. The second stage involves the reduction of the stored NO$_X$ to N$_2$ using a very short rich period. The cycle is repeated to achieve more than 90% conversion of exhaust NO$_X$ [6]. There is a fuel penalty when the engine shifts from lean to rich mode [7]. During the lean mode of operation, the NO in the exhaust is oxidized over precious metals such as Pt or Rh to NO$_2$ which then reacts/stores over a base metal oxide such as BaO until an unacceptable amount of NO$_X$ is released to the atmosphere because of saturation of accessible storage sites. During the rich cycle, a short burst of hydrocarbon, CO and/or hydrogen then reduces the stored NO$_X$ to N$_2$. Typically, some NO$_X$ desorbs during the initial part of the regeneration and is coined the "NO$_X$ puff".

In order to design a catalyst that meets the requirements of NO_X reduction, it is necessary to understand the transient mechanisms of NO_X storage, reduction and of major byproduct formation. Precious metals such as Pt and Rh are extensively used because of their activity in the oxidation of NO to NO_2 (Pt), the storage of NO_2 to nitrites and nitrates, and the reduction of NO to N_2 (Pt and Rh). However, the undesired reduction of NO by H_2 to N_2O or NH_3 remains a challenge. N_2O, a greenhouse gas, is produced at lower temperature during reduction on Pt in particular, while NH_3 is formed under conditions having a surplus of H_2. On the other hand, H_2 is known to be the most effective reductant of gas phase or stored NO_X, and as a result there are efforts to maximize its formation by steam reforming and water gas shift chemistries [8,9]. In the current study we focus on the performance of Pt in the absence of the BaO storage component in order to better understand mechanistic and product distribution issues.

Transient studies of catalytic reactions provide useful mechanistic and kinetic information. Temporal analysis of products (TAP) [10,11] has proven its utility in a host of catalytic reaction systems ([12] and references within). It is particularly suited for NO_X storage and reduction which is an inherently transient catalytic process. Recently TAP was used to study NSR in order to elucidate mechanistic pathways and provide transient data for micro-kinetic modeling [13,14]. The TAP reactor is operated at pressures low enough that Knudsen diffusion is the dominant transport process. Moreover, the rates are sufficiently low that operation is isothermal. These features are desirable since they simplify the interpretation of the experimental data. In previous studies the TAP reactor has been configured with one zone or three zones. In the three-zone configuration the active catalyst is sandwiched between inert solid particles. Efforts have been made to reduce the thickness of the catalyst zone [15] or to use a point source [16] to minimize concentration gradients along the catalyst zone. In this study we use an alternative three-zone monolith configuration which shows an improvement in the response in terms of the elution of the pulsed gas. An additional advantage of using the monolith catalyst is for direct comparison to performance in a standard atmospheric pressure flow reactor.

The main objective of the current work is to gain mechanistic insight about NO decomposition and NO reduction by H_2 on Pt/Al_2O_3 powder and Pt/Al_2O_3 washcoated monolith. This study builds on our recent TAP study of the same reaction on Pt/BaO/Al_2O_3 but focuses exclusively on the Pt catalyst, reactivity and selectivity in the absence of the BaO. The transient data provide salient information about the mechanism and kinetics of NO reduction by H_2 on Pt/Al_2O_3 catalyst through measurement of product distributions over a range of conditions. We also compare the results of the three-zone catalyst powder to three-zone monolith catalyst of the same Pt loading. To this end, the advantages of using the monolith in the TAP are demonstrated.

2. Experimental

A Generation-1 TAP reactor system was used following the methodologies described in more detail elsewhere [13]. Experiments were carried out on 1.52 wt% Pt/Al_2O_3 powder and monolith catalysts, each having 30.4% Pt dispersion, 1.14 m^2 exposed Pt/g catalyst (powder or washcoat) and 3.7 nm average Pt particle diameter. The catalyst samples were provided by BASF Catalysts LLC (Iselin, NJ). About 90 mg of the powder catalyst (powder particle diameter typically less than 50 μm), having about 1.2×10^{18} exposed Pt sites, was sandwiched between two zones containing inert quartz beads (250–300 μm diameter), forming a three-zone powder configuration (Fig. 1(c)) in a cylindrical reactor of 42 mm length and 5.3 mm diameter. The thicknesses of two inert zones were 24 mm and 12 mm while the sandwiched powder zone was
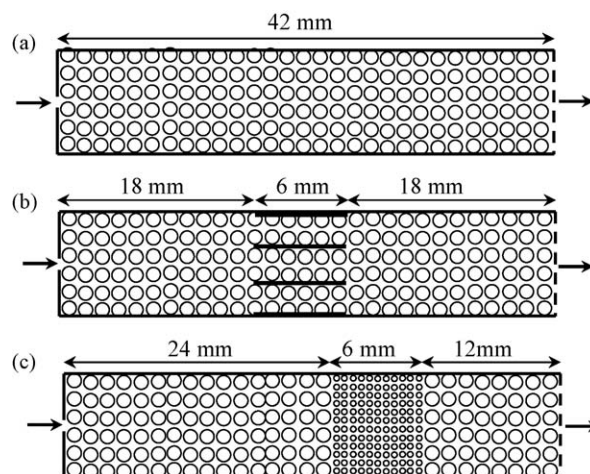

Fig. 1. Schematics of one-zone inert (a), three-zone monolith (b), and three-zone powder (c) configurations.

6 mm thick which is sufficiently thin to ensure isothermal operation. The cordierite monolith catalyst had a length of 6 mm with 3×3 channels, containing about 1.2×10^{17} exposed Pt atoms. The monolith had a cell density of 400 channels/in.^{2}, while the measured average cordierite wall thickness and washcoat thickness were approximately 177 μm and 15 μm, respectively. The monolith was placed between two symmetrical inert zones (18 mm each) in the reactor with inert beads filling the channels as well as the void space between monolith wall and reactor wall (Fig. 1(b)). (Remark: Zheng et al. [16] used a single Pt particle comprising 0.3% of the cross-sectional area of the TAP micro-reactor and reported 95% conversion. It indicates that possible gas bypass should be insignificant in the case of monolith.) Typically, 10–15 inert beads are present in a cross section of one channel. The washcoat of the monolith catalyst had the same composition and dispersion as the powder catalyst. The 6 mm length of the monolith was sufficient to ensure a uniform temperature. In a typical experiment, the catalyst was first reduced with H_2 for 2 h at 400 °C, and was then brought down to reaction temperature (150, 250, or 350 °C). Unlike atmospheric pressure operation in which typical NO and H_2 molar concentrations do not exceed ca. 1000 ppm or 2%, respectively, pure components are used in the TAP studies. The maximum pressure in the reactor can exceed 1 mbar in the front of inert zone just at the time of pulsing, but the pressure decays sharply in space and time [17]. The partial pressures of the NO and H_2 over catalyst zone during a pulse in the TAP do not exceed about 10^{-2} Torr (0.01 mbar), which compares to 1 and 20 mbar, respectively, during atmospheric pressure operation. For this reason external transport limitations are not likely to be encountered during normal TAP operation.

Effluent species including unreacted NO, and products N_2O, N_2, NH_3, and H_2O were monitored with a calibrated UTI 100C quadrupole mass spectrometer. Calibration numbers for different gaseous species were estimated using a one-zone inert bed reactor. This involved feeding several hundred pulses of species including N_2, H_2, O_2, NO, N_2O, etc. to the inert bed. The number of molecules per pulse was calculated using changes in pressure of the isothermal and isochoric bulb for each gaseous species. The exit responses of the pulses were measured by the mass spectrometer. The integral area of exit response was correlated to the fed molecules by the calibration number. Calibration numbers for NH_3 and H_2O were calculated from N and O balances, respectively, for selected experiments on Pt/Al_2O_3 catalysts and used throughout the analysis. Typically, the mass balances with these calibration numbers have accuracy within 10%. Two principal reaction types were carried out, which are described below. Calibration of NO_2
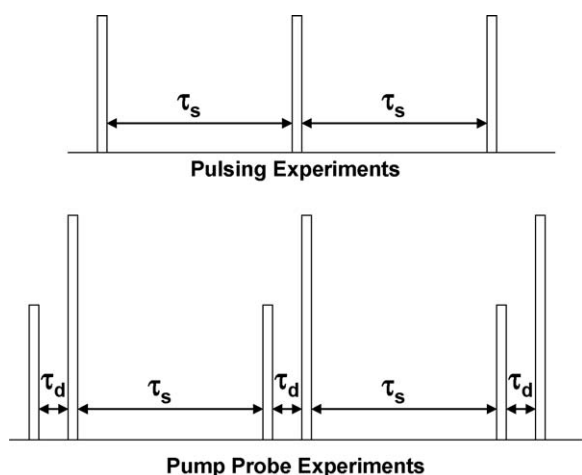
Fig. 2. Schematics of delay time (τ_d) and spacing time (τ_s) for pulsing experiments and pump-probe experiments.

was not carried out because NO_2 (m/e = 46) was not detected in the effluent under any conditions. NO_2 decomposition within the mass spectrometer can be ruled out because there was no detectable O_2 (m/e = 32). Only if NO_2 was fed to an inert catalyst bed was it detected, as reported previously by Kabin et al. [13].

2.1. NO pulsing experiments

These experiments involved the exposure of a large number of NO pulses to the pre-reduced three-zone powder or monolith catalyst with a fixed spacing time, τ_s (Fig. 2). In these experiments the typical size of NO pulse was $1.0–3.0 \times 10^{16}$ molecules/pulse. The larger pulse size may cause a deviation of the species transport from Knudsen diffusion regime. But, such deviations do not pose any problem for our qualitative analysis. Unless otherwise stated, the spacing time between each pulse was 9 s. The pulsing was carried at 150, 250 and 350 °C. Overall reactions occurring during NO decomposition are:

$2NO \rightarrow N_2 + O_2$

$2NO \rightarrow N_2O + 0.5O_2$

$2NO \rightarrow NO_2 + 0.5N_2$
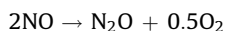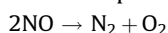
2.2. NO–H$_2$ pump-probe experiments

In NO–H_2 pump-probe experiments, pulses of NO and H_2 were sequentially fed to the catalyst. As depicted schematically in Fig. 2, the duration between successive H_2 and NO pump-probe cycles is the "spacing time" (τ_s) while the time duration between the NO and H_2 pulses of a single cycle is the "delay time" (τ_d). In a typical NO–H_2 pump-probe experiment, τ_d was fixed between 0.0 s and 1.0 s while τ_s was fixed at 9.0 s. The NO and H_2 pulse intensities were varied by the opening time (200–500 μs) of each pulse valve. The NO–H_2 pump-probe was carried at three different temperatures with different H_2 to NO ratios to assess the temperature and concentration effects. The three primary overall reactions between NO and H_2 are:

$NO + 0.5H_2 \rightarrow 0.5N_2O + 0.5H_2O$

$NO + 1.0H_2 \rightarrow 0.5N_2 + H_2O$

$NO + 2.5H_2 \rightarrow NH_3 + H_2O$
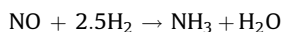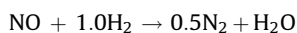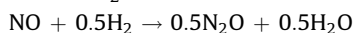
We define the feed ratio H_2/NO = 1 for the production of N_2. Thus for $H_2/NO < 1$, H_2 (NO) is the limiting (excess) reactant while for $H_2/NO > 1$, NO (H_2) is the limiting (excess) reactant.

3. Results

3.1. Comparison of transport properties of powder and monolith catalysts

In order to compare the transport of a non-interacting gas over inert beads, catalytic monolith and catalyst powder, three reactor configurations were used. The first reactor was filled with inert beads, called one-zone inert configuration (Fig. 1(a)). For the second configuration, a 6 mm monolith piece with 3×3 channels was placed in the middle of the reactor. The void space in the channels was filled with inert beads. It is referred to as three-zone monolith configuration (Fig 1(b)). The third configuration, called the three-zone powder configuration (Fig. 1(c)), consisted of powder catalyst sandwiched between two inert zones. The reactor dimensions were fixed (length 42 mm × diameter 5.3 mm) in all three configurations, so the amount of inert beads used in the three-zone powder and monolith configurations was less than the amount used in the one-zone inert configuration.

Argon ($1.0–2.0 \times 10^{15}$ molecules/pulse) was pulsed over the three configurations with 3 s spacing time at 150 °C. The height normalized transient responses are plotted in Fig. 3. Note that the solid lines depict the actual profiles while symbols are used to distinguish different curves. The exit transient profiles for three-zone monolith and one-zone inert configuration were nearly identical with the pulse response much sharper than the three-zone powder configuration. A closer inspection indicates that the residence time of Ar in the three-zone monolith is slightly shorter than in the one-zone inert configuration. This difference can be attributed to the decrease in radial diffusivity in monolith region. Moreover, Knudsen diffusion transport was confirmed for one-zone inert and three-zone monolith by peak flux and peak time product criteria ($J_p t_p = 0.31$) for area normalized curve [18]. There is no simple Knudsen diffusion criterion for three-zone powder configuration. Clearly, the broader profile of three-zone powder configuration is due to a lower effective diffusivity in the sandwiched powder zone. We discuss this point in more detail in the Section 4.

3.2. Powder catalyst

3.2.1. NO pulsing at 150–350 °C
NO uptake over Pt/Al_2O_3 at 150, 250 and 350 °C shown in Fig. 4 exhibits similar trends for NO uptake on Pt/BaO/Al_2O_3 at 350 °C, as reported previously [14]. N_2 is produced during the first 30–40 NO
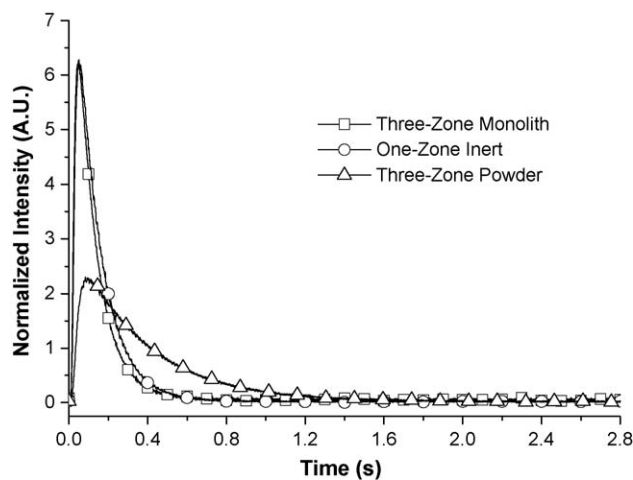

Fig. 3. Area normalized transient response of argon on three-zone monolith, one-zone inert and three-zone powder configurations at 150 °C. The solid lines depict the actual profiles while symbols are drawn to distinguish different lines in all plots in this paper.
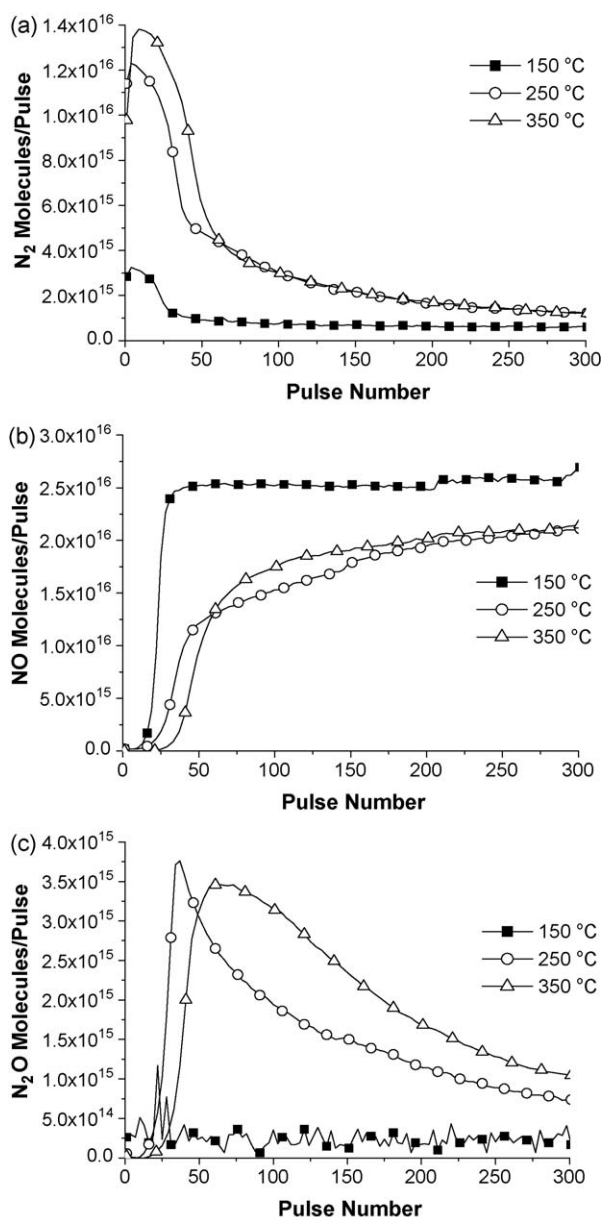
Fig. 4. N_2 (a), NO (b) and N_2O (c) profiles for NO pulsing experiments on Pt/Al_2O_3 powder catalyst with inlet NO pulse size of {2.8, 2.7, 2.5} $\times 10^{16}$ molecules/pulse at {150, 250, 350} °C, respectively.

pulses in this temperature range without breakthrough of NO, where breakthrough is defined as the point of inflection of the NO response. NO breakthrough commenced at about the 35th and 45th pulse for catalyst temperatures 250 and 350 °C, respectively. The earlier breakthrough for NO at 250 °C is due in part to the slightly larger pulse size (2.7×10^{16} at 250 °C vs. 2.5×10^{16} at 350 °C) although, as we discuss later, there may be a difference in the extent of coverage by non-dissociated NO and O adatoms resulting from NO decomposition. At the lower temperature (150 °C), a fairly sharp breakthrough of NO is observed at about the 20th pulse (NO = 2.8×10^{16} molecules/pulse). The production of N_2 at 250 and 350 °C is almost in stoichiometric proportion (N_2 production is about one-half that of NO pulse size), while at 150 °C the N_2 production is far below what would be expected stoichiometrically. A negligible amount of N_2O was produced at 150 °C while at higher temperatures the N_2O production is more significant and peaks at the point of NO breakthrough. Its production then falls monotonically.

There was no evidence for NO_2 formation during the NO pulsing experiments based on the absence of the m/e = 46 peak. In fact, in a series of experiments (not shown here) involving NO_2 pulsing over the Pt/Al_2O_3 catalyst in the temperature range 200–400 °C, NO_2 readily decomposes and only NO, O_2 and N_2 were seen in the effluent. Since O_2 was not observed during any of the NO pulsing or NO–H_2 pump-probe experiments, the possibility of formation of NO_2 as product was ruled out.

An examination of the effluent species transient profiles for NO and N_2 provides more detailed information about the kinetics of NO decomposition. Example data are shown in Fig. 5 for the NO pulsing experiment at 150 °C. The initial NO pulses adsorb completely on the Pt catalyst, hence NO (NO pulse 2nd and 8th) is not seen in the effluent. The adsorbed NO partially decomposes to form N_2 during initial pulses (N_2 pulses 1st and 7th). In fact, the first pulse gives the highest production of N_2. With the increase in pulse number, the peak height of N_2 decreases and eventually effluent peak becomes more difficult to discern as the N_2 signal approaches a baseline level. Not until the 16th pulse does unreacted NO appear in the reactor outlet. This suggests that a large fraction of NO adsorbs on the Pt and/or alumina support, recalling that the N_2 produced is far less than the stoichiometric amount. Though N_2 being a product, it comes out of the reactor earlier than NO because of NO readsorption and slow desorption. The NO effluent shows a definitive peak which increases with pulse number. However, NO elutes much more slowly out of the reactor than N_2, which is attributed to the slower desorption of NO from the catalyst.
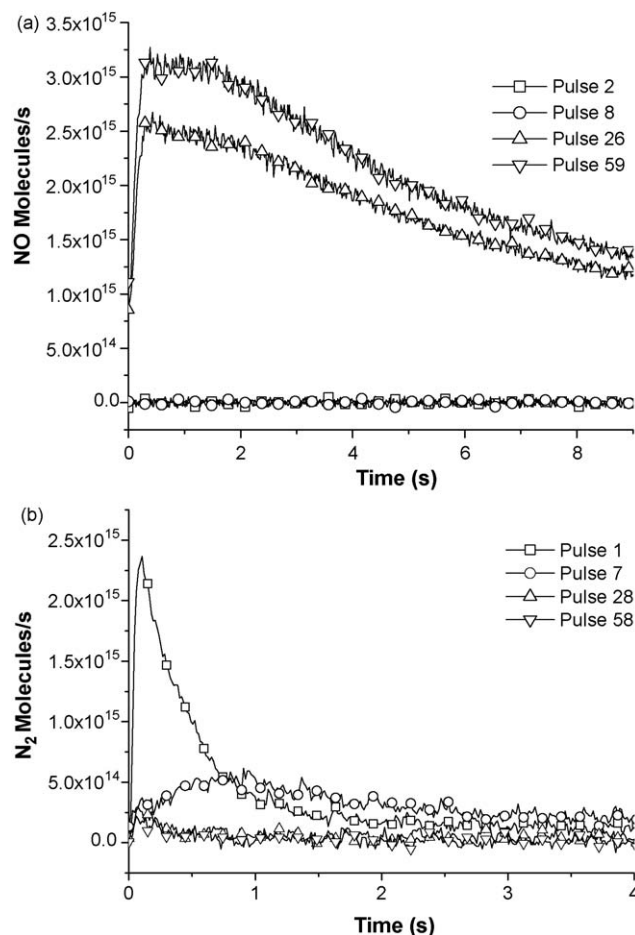

Fig. 5. Individual transient pulse profiles for NO (a) and N_2 (b) pulses for powder catalyst at 150 °C.
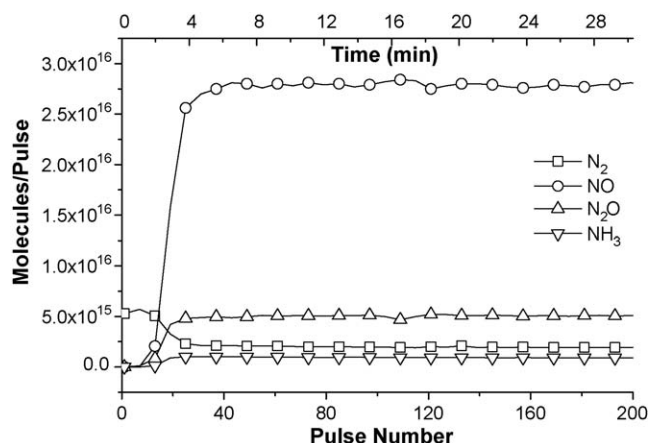
Fig. 6. NO–H_2 pump-probe experiment on Pt/Al_2O_3 powder catalyst at 150 °C. H_2/NO ratio was maintained at 0.3 (excess NO) with $NO_{in} = 4.2 \times 10^{16}$ and $H_{2,in} = 1.3 \times 10^{16}$ having delay of 0.1 s and spacing 9.0 s.

3.2.2. NO–H_2 pump-probe at 150–350 °C

Pump-probe experiments reveal the transient reaction between NO and H_2 which results in a product distribution that depends on the temperature, the H_2/NO ratio, and the delay time between the NO and H_2 pulses. In the first set of experiments carried out at 150 °C, the delay time τ_d was maintained at 0.1 s. Fig. 6 shows the results for H_2/NO = 0.3. The data have some trends similar to NO pulsing on Pt/Al_2O_3 (Fig. 4) in terms of the NO and N_2. But there are clear differences. Both the N_2 and N_2O production are sustained at levels above the baseline after NO breakthrough occurs. In addition, a small amount of NH_3 is observed in the product. When H_2/NO ratio is increased to 2.6, while maintaining a temperature of 150 °C, a shift in the product distribution is encountered (Fig. 7). N_2 production remains at low level (less than 20% of NO input) while the major product is NH_3. The late arrival of NH_3 in the product is undoubtedly due to its slow desorption from the catalyst. The N_2O production is negligible in the presence of excess H_2.

When the temperature is increased to 350 °C for a feed containing excess NO (H_2/NO = 0.39) the production of N_2 achieves its maximum value during the initial pulses, then decreases to a low but non-zero level by the 1000th pulse (Fig. 8). Most of the hydrogen fed in this experiment is consumed since it is the limiting reactant. The N_2 and N_2O produced approach constant, non-zero

Fig. 7. NO–H_2 pump-probe experiment on Pt/Al_2O_3 powder catalyst at 150 °C. H_2/NO ratio was maintained at 2.6 (excess H_2) with $NO_{in} = 2.8 \times 10^{16}$ and $H_{2,in} = 7.1 \times 10^{16}$ having delay of 0.1 s and spacing 9.0 s.
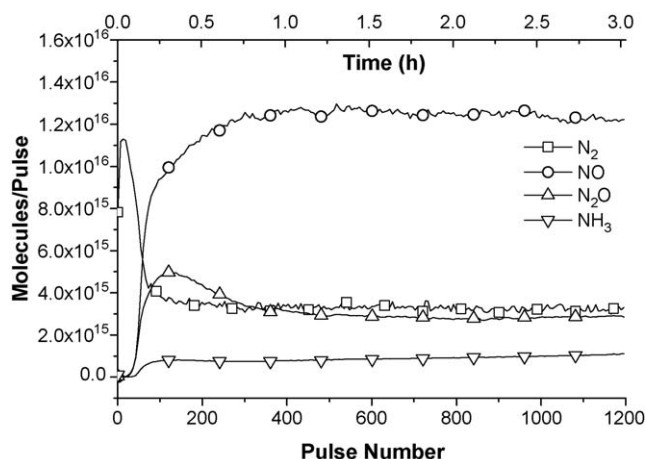

Fig. 8. NO–H_2 pump-probe experiment on Pt/Al_2O_3 powder catalyst at 350 °C. H_2/NO ratio was maintained at 0.39 (excess NO) with $NO_{in} = 2.5 \times 10^{16}$ and $H_{2,in} = 9.6 \times 10^{15}$ having delay of 0.1 s and spacing 9.0 s.

levels while a small amount of NH_3 is sustained under these conditions. It is noted that for every three molecules of H_2 consumed, there are about four molecules of NO consumed (or 1 N_2 and 1 N_2O formed), which corresponds well with the stoichiometric reduction of NO to N_2 and N_2O. NO breakthrough occurs because of oxygen poisoning of the Pt surface due to insufficient H_2 and approaches a sustained level.

Fig. 9 compares the selectivities of N_2 and NH_3 produced to NO fed under excess H_2 conditions (H_2/NO = 2.2–2.6) at three
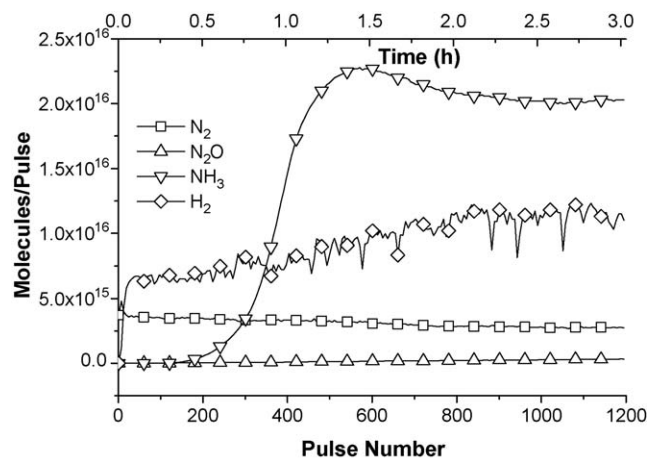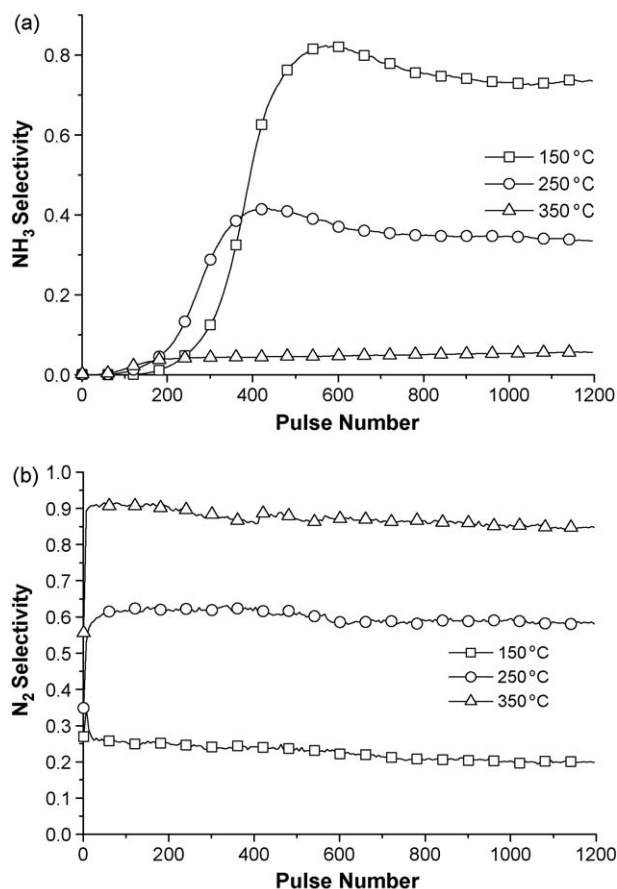

Fig. 9. NH_3 (a) and N_2 (b) selectivities for NO–H_2 pump-probe in case of excess H_2 on powder Pt/Al_2O_3 with varying temperature at delay time of 0.1 s and spacing 9.0 s.
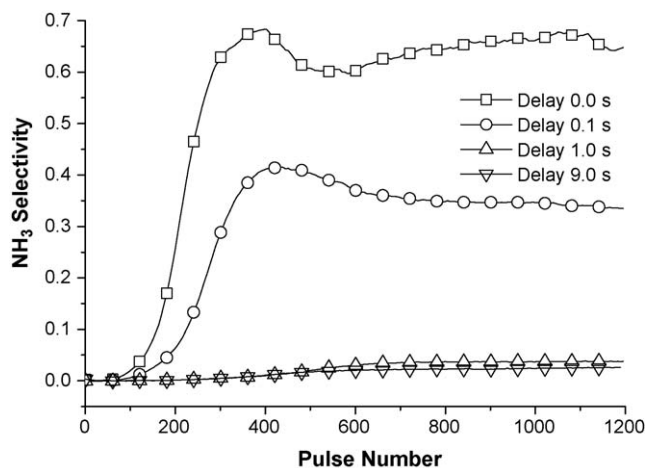
Fig. 10. Ammonia selectivity for NO–H_2 pump-probe experiments at 250 °C in case of excess H_2 on powder Pt/Al_2O_3 with different delay times.

Fig. 12. N_2, NO and N_2O profiles for comprehensive NO pulsing experiment on Pt/Al_2O_3 monolith catalyst from 150 °C to 350 °C. NO pulsing was stopped at 1400th pulse.

3.3. Monolith catalyst

3.3.1. NO pulsing at 150–350 °C

different temperatures. At sustained level of N_2 and NH_3 (beyond the 800th pulse), the selectivity is highest for ammonia at 150 °C but highest for N_2 at 350 °C. In an independent experiment not shown here, NH_3 decomposition did not exceed 15% at 350 °C. This rules out increased N_2 observed at higher temperatures via ammonia decomposition. Rather, the selectivity trend is indicative of the rate of NO decomposition at higher temperature playing a larger role at higher temperature for the particular delay time between the NO and H_2 pulses, which we elaborate on next.

The NH_3 selectivity is a sensitive function of the delay time between the NO and H_2 pulses. Fig. 10 shows the production of NH_3 in excess H_2 (H_2/NO = 2.0–2.8) at 250 °C for delay times 9 s, 1 s, 0.1 s and 0 s (i.e., "mixed feed" with both valves opened at the same time). A progressively decreasing production of NH_3 is observed with increasing τ_d. For example, for delay times of 1 s and 9 s, the amount of NH_3 produced approaches the detectable limit. The observation is similar for other temperatures. Fig. 11 shows the integrated NH_3 selectivity for three different temperatures at different delay times. It is seen that the largest amount of NH_3 is produced at the lowest temperature and the "mixed" feed. These trends are discussed in Section 4.
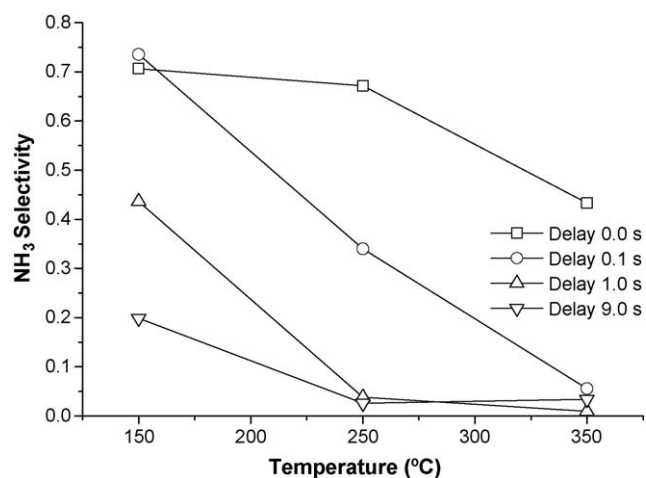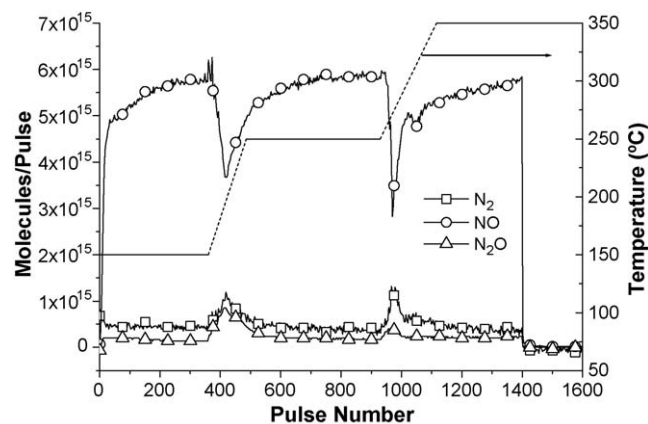

Fig. 11. Plot of ammonia selectivity for NO–H_2 pump-probe experiments with excess H_2 on powder Pt/Al_2O_3 as a function of temperature with delay time as parameter.

Similar NO pulsing experiments were repeated using the monolith catalyst over the same range of temperature. Fig. 12 shows an experiment in which NO pulsing was sustained over the entire 150–350 °C range with spacing time of 9 s and an average of 7.3×10^{15} molecules/pulse. At the start of the experiment when the temperature was the lowest (150 °C), NO pulsing on the Pt/Al_2O_3 monolith resulted in a small amount of N_2 formed during the initial few pulses followed by the sharp breakthrough of NO. After the constant integral profiles were attained at the 360th pulse, the monolith temperature was ramped to 250 °C. A sharp decrease in the NO flux was observed. This was accompanied by an increase in the production of N_2 and N_2O attributed to an increase in the rate of NO decomposition. Eventually, the integral NO flux increased to a constant value while the integral N_2 and N_2O production rates decreased to constant levels. A similar response in the NO, N_2 and N_2O fluxes was observed during a temperature ramp from 250 °C to 350 °C at the 930th pulse. As shown in the figure, at the 1400th pulse, the NO pulsing was stopped that caused N_2, NO and N_2O profile to reach at a base level. This experiment shows that as temperatures increased, the rate of NO decomposition increased. Moreover, since the monolith catalyst was reduced only at the beginning of the experiment, the accumulation of oxygen on the catalyst was progressive throughout the experiment. Thus, the N_2 production did not approach the stoichiometric value due to significant oxygen poisoning. We expand on this point in reference to the microkinetics in Section 4.

Transient profiles for NO and N_2 for the NO pulsing experiment at 150 °C on the three-zone monolith catalyst are shown in Fig. 13. The NO and N_2 exit flux profiles are similar to the transient profiles for the powder catalyst (Fig. 5), but the NO profile is much sharper and declines more rapidly for monolith catalyst than the corresponding response for the powder catalyst. This feature makes the monolith data more amenable to a quantitative kinetic analysis. We return to this point in Section 4.

3.3.2. NO–H_2 pump-probe at 150–350 °C

NO–H_2 pump-probe experiments were carried out for the monolith catalyst. The delay time between NO and H_2 pulse was kept at 0.1 s while the spacing time between successive H_2 and NO pairs was fixed at 9 s (Fig. 14). In this experiment about 2000 total pulses were injected with the temperature maintained at three levels (150, 250, 350 °C). The NO and H_2 pulse intensities were 8.3×10^{15} and 3.8×10^{16}, respectively (H_2/NO = 4.6). Similar to
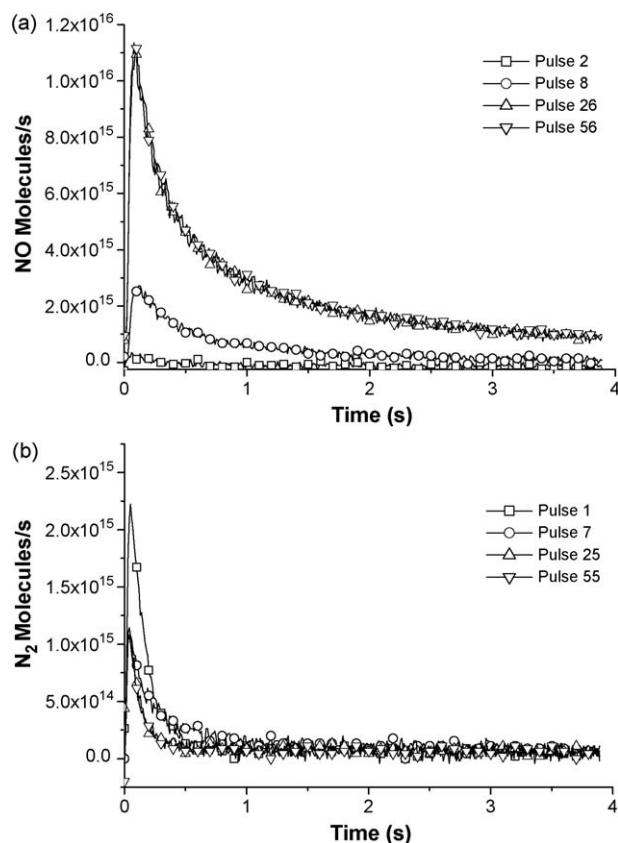
Fig. 13. Individual transient pulse profiles for NO (a) and N_2 (b) pulses for three-zone monolith configuration at 150 °C.

NO–H_2 pump-probe on the powder catalyst at 150 °C, NH_3 and H_2O were the major products while N_2 and N_2O production remain at low levels. The temperature was ramped from 150 °C to 250 °C at the 600th pulse. A sharp effluent "puff" of NH_3 and H_2O indicated an accumulation of H_2O and NH_3 on the monolith catalyst at 150 °C. After sustained integral profiles were reached at 250 °C, another ramp in temperature to 350 °C at the 1200th pulse resulted in a "puff" of NH_3 and H_2O, but the increase was not as large as the one at lower temperature, indicating in part less accumulation at the higher temperature. This experiment with excess H_2 further suggests that NH_3 formation declines with an increase in temperature and the decline in NH_3 is compensated by a corresponding increase in N_2 production.
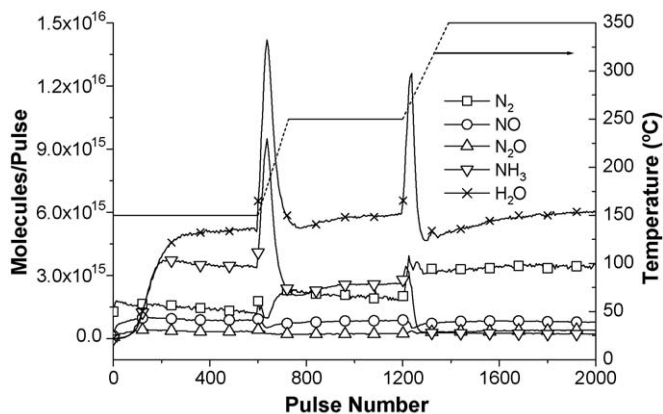

Fig. 14. Comprehensive NO–H_2 pump-probe experiment over Pt/Al_2O_3 monolith from 150 °C to 350 °C with delay time of 0.1 s and 4 s spacing. H_2/NO ratio was maintained at 4.6 (excess H_2) with $NO_{in} = 8.3 \times 10^{15}$ and $H_{2,in} = 3.8 \times 10^{16}$.
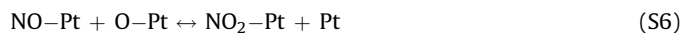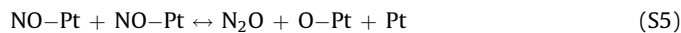
4. Discussion

We have carried out NO pulsing and NO–H_2 pump-probe over Pt/Al_2O_3 powder and monolith catalysts having the same Pt loading and dispersion. Comparisons have been made between the powder and monolith in terms of the NO decomposition and reduction of NO with H_2 as well as transport processes. In this section we expand on the main findings in terms of mechanistic implications for both reaction systems and the transport behavior of the monolith and powder catalysts.

4.1. NO decomposition

The possible products that can form during NO decomposition are N_2, O_2, N_2O, and NO_2. Oxygen binds to Pt strongly and does not appreciably desorb below 400 °C because of its high binding energy (200–240 kJ/mol). Adsorbed oxygen covers the Pt surface and inhibits further reactions.

There was no evidence for NO_2 formation during the NO pulsing experiments but its formation as a surface intermediate cannot be ruled out. During the latter part of a multi-pulse NO experiment the data suggest that the Pt surface is covered with O or NO (at lower temperature). Consequently, during a pulse of NO, any NO that adsorbs may react with O adatoms to form NO_2. Zhou et al. [19] reported that gas phase NO_2 may undergo equilibration with NO and O_2 prior to reaching the mass spectrometer. However, as stated earlier, no NO_2 or O_2 was detected during the NO pulsing. This suggests that the desorption of any adsorbed NO_2 is negligible. On the other hand, during isotopic ^{15}NO–$^{18}O_2$ pump-probe experiments (not shown here), while $^{15}NO_2$, $^{15}NO^{18}O$ and $^{15}N^{18}O_2$ were not observed, O_2 and $O^{18}O$ were detected. This finding suggests that $^{15}NO_2$ and $^{15}NO^{18}O$ may form as intermediates during ^{15}NO exposure to the O/^{18}O covered Pt surface, but it quickly decomposes, forming O_2 and $O^{18}O$.

The results for NO decomposition are consistent with those of our earlier study on Pt/BaO/alumina powder at 350 °C [14]. These additional data over a wider range of temperatures help to elucidate the reaction pathways for NO decomposition on Pt. Based on earlier studies, an accepted mechanism for NO decomposition on Pt follows steps (S1)–(S5) [14,20,21]:

$$NO + Pt \leftrightarrow NO–Pt \tag{S1}$$

$$NO–Pt + Pt \leftrightarrow N–Pt + O–Pt \tag{S2}$$

$$N–Pt + N–Pt \rightarrow N_2 + 2Pt \tag{S3}$$

$$N–Pt + NO–Pt \leftrightarrow N_2O + 2Pt \tag{S4}$$

$$NO–Pt + NO–Pt \leftrightarrow N_2O + O–Pt + Pt \tag{S5}$$

$$NO–Pt + O–Pt \leftrightarrow NO_2–Pt + Pt \tag{S6}$$

$$NO_2–Pt \leftrightarrow NO_2 + Pt \tag{S7}$$

Although, the data do not indicate that NO_2 is a gas phase product during sequential pulses of NO, it may form as an intermediate via step (S6). The desorption of NO_2 (step (S7)) is shown for completeness.

The rate of NO decomposition increases with temperature and the degree of reduction of the Pt surface. All of the NO pulsing experiments show that the rate is highest when the Pt surface is fully reduced and devoid of surface oxygen, and that the rate declines as oxygen adatoms are deposited onto the surface (Fig. 4). At 350 °C the reaction is nearly stoichiometric during the initial pulses. However, at 150 °C the NO decomposition rate is much lower. This suggests that NO bond scission is insignificant based on

the relatively low amount of N_2 formed. If each NO molecule occupies a single Pt site, the number of NO pulses needed to completely saturate the Pt surface is 43, 44 and 48 at 150, 250 and 350 °C, respectively. But, the actual NO breakthrough occurs around the 20, 35 and 45th pulse, respectively at these temperatures. This suggests that each NO molecule occupies two Pt sites at 150 °C when the NO decomposition is negligible. The above observation is in good agreement with NO adsorption study on Pt(1 0)-(1 × 2) [22] which showed that NO molecularly adsorbs on Pt in a bridge and linear configuration at low and high NO exposure, respectively. At 150 °C, the absence of NO decomposition enables the NO to remain on Pt in the bridge form, occupying two Pt sites, and the NO breakthrough here is an indication of nearly complete coverage of Pt by bridge-bonded NO. The accumulation of NO further suggests that the rate of NO bond scission (step (S2)) becomes limiting at 150 °C. In contrast, at the higher temperature (350 °C) adsorbed NO decomposes to form N_2, leaving O adatoms on the surface. Hence the NO breakthrough point at higher temperature is an indication of nearly complete coverage on Pt by O adatoms with the remaining sites covered by adsorbed N and NO species. We will return to this observation in the analysis of the NO–H_2 pump-probe experiments.
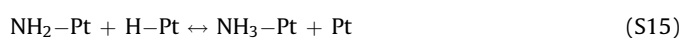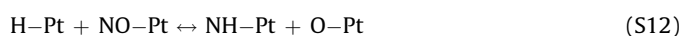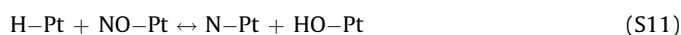
NO pulsing on Pt/Al_2O_3 monolith catalyst with an intermittent temperature ramp further confirms the above findings of the constant temperature experiments. The monolith experiment in Fig. 12 shows that during the initial few pulses of NO at 150 °C, N_2 is produced well below its stoichiometric amount and therefore most of NO adsorbs without decomposition. This leads to an accumulation of NO in addition to O during the initial part of the experiment. This is followed by a sharper and earlier NO breakthrough, verifying that each NO occupies multiple sites or excludes adsorption on neighboring vacant sites. When the temperature is ramped to 250 °C at the 360th pulse, a sharp decrease in effluent NO is observed due to conversion of bridge-bonded NO or linear-bonded NO on Pt, creating vacant sites for further NO adsorption. The adsorbed NO dissociates, forming N and O adatoms, which leads to an increase in N_2 and N_2O production. The NO dip and the N_2 and N_2O peaks coincide. The NO effluent profile gradually increases to a constant level. A further temperature ramp to 350 °C at the 930th pulse has a similar effect on the NO, N_2 and N_2O profiles. With increasing temperature, the sites that were previously occupied by adsorbed NO and/or O become vacant for additional NO adsorption and decomposition, leading to an increased amount of N_2 and N_2O products. The return of the NO effluent flux to a constant level suggests that surface sites become occupied and the NO decomposition rate decreases to a low, but non-zero level.

The decomposition of NO was sustained on the Pt catalyst even though the number of oxygen atoms produced during the production of N_2 and N_2O exceeded the number of exposed Pt sites. Similar findings were reported by Medhekar et al. [14] on Pt/Al_2O_3 and Pt/BaO/Al_2O_3. Independent O_2 pulsing experiments carried out on the same Pt/Al_2O_3 catalyst resulted in an oxygen uptake that is 3–4 times the number of exposed Pt sites. Previous high vacuum studies on single crystal Pt or polycrystalline Pt catalysts result in an atomic oxygen coverage of 0.25 ML [23]. Oxygen coverages exceeding 0.25 ML have been successfully generated on Pt under UHV conditions using aggressive molecular oxidants like NO_2 [24], O_3 [25], and more recently, gaseous oxygen atoms [26]. Atomic oxygen coverages as high as 2.9 ML could be generated on Pt(1 1) using an atomic oxygen beam [26]. Putna et al. [27] showed that the oxygen coverage also depends on the Pt particle size; for example, it increased by threefold when the Pt particle size was reduced to 2.0 nm. Shaikhutdinov et al. [28] observed that the O coverage at 400 K on Pd supported on thin film of alumina achieved a level corresponding to approximately four O

atoms per Pd surface atom. The oxygen uptake was an order of magnitude higher than the saturation coverage of a Pd(1 1) single crystal surface at the same temperature. The investigators described diffusion processes during oxygen exposure, which involve either oxygen diffusion into the Pd particles and/or diffusion of adsorbed oxygen atoms into the alumina support. They further showed that oxygen treatment modifies the specific long range order of alumina film in the presence of the precious metal. This indicates that alumina too may store some oxygen in presence of precious metal. The diffusion processes on precious metals and support as well as smaller Pt particle size (3.7 nm) may lead to higher oxygen uptake on the Pt/Al_2O_3 during the NO decomposition and oxygen pulsing experiments. Moreover, some oxygen may desorb from Pt below 400 °C. Each of these factors lead to a sustained production of N_2 and N_2O during prolonged NO pulsing on powder and monolith catalysts.

4.2. NO–H_2 pump-probe

The NO–H_2 pump-probe experiments add a rich complexity of surface chemistry with multiple products formed. These experiments resulted in the formation of NH_3 and H_2O in addition to N_2 and N_2O. The following set of reaction steps will be used to explain the trends in the data:

$$H_2 + 2Pt \leftrightarrow 2H-Pt \tag{S8}$$

$$H-Pt + O-Pt \leftrightarrow OH-Pt + Pt \tag{S9}$$

$$H-Pt + OH-Pt \leftrightarrow H_2O + 2Pt \tag{S10}$$

$$H-Pt + NO-Pt \leftrightarrow N-Pt + HO-Pt \tag{S11}$$

$$H-Pt + NO-Pt \leftrightarrow NH-Pt + O-Pt \tag{S12}$$

$$N-Pt + H-Pt \leftrightarrow NH-Pt + Pt \tag{S13}$$

$$NH-Pt + H-Pt \leftrightarrow NH_2-Pt + Pt \tag{S14}$$

$$NH_2-Pt + H-Pt \leftrightarrow NH_3-Pt + Pt \tag{S15}$$

$$NH_3-Pt \leftrightarrow NH_3 + Pt \tag{S16}$$

Reaction steps (S8)–(S10) comprise H_2 oxidation to H_2O. Reaction step (S9) is the key scavenging reaction that cleans the Pt surface during the pump-probe experiments. Reactions (S11) and (S12) involve NO bond scission through reaction with H–Pt. Reactions ((S13)–(S16)) are those involved in the formation of NH_3.

The lower production of N_2O at 150 °C during NO pulsing on Pt/Al_2O_3 suggests two factors: Either there is insufficient N–Pt species because of a low NO decomposition rate (step (S4)) or the NO disproportionation (step (S5)) is rate limiting at this temperature. If we compare the NO decomposition (Fig. 4) to the NO–H_2 pump-probe at 150 °C in excess NO (Fig. 6), we observe that N_2O formation is sustained at a higher level in the latter experiment. The formation of N_2 during NO decomposition is similar to N_2 formation during the NO–H_2 pump-probe experiments at 150 °C. This indicates that its formation is not affected by the extent to which H_2 scavenges the surface oxygen. On the other hand, the formation of N_2O during the pump-probe indicates that the hydrogen adatoms react with surface oxygen to provide additional Pt sites for adsorbed NO to decompose, forming N–Pt species, and then ultimately N_2O. Alternatively, the H–Pt may react directly with adsorbed NO species, extracting an O from the NO, giving N–Pt species. This reaction step was originally proposed by Hecker and Bell [29] in their study of NO reduction by H_2 over silica-supported rhodium. This reaction sequence is also consistent with

a study by Smirnov et al. [30], who used HREELS to study the NO + H reaction on Pt(1 1). They reported evidence for a HNO_{ad} intermediate from the reaction of H adatoms with bridge-bound NO_{ad}, and subsequent reaction of HNO_{ad} with surface H to form N adatoms. Ford et al. [23] calculated that NOH_{ad} is a more stable intermediate than HNO_{ad} during NO reduction by H_2 to form N_{ad}. We earlier concluded from the NO pulse experiments at 150 °C that most of the NO is present in molecular form since negligible production of N_2O and N_2 occurred. Taken together, this suggests that in the presence of a limiting amount of H_2 during the NO–H_2 pump-probe experiment, the higher N_2O production rules out the disproportionation route to N_2O (step (S5)) compared to NO–Pt reacting with N–Pt (step (S4)). Sufficient hydrogen adsorbs and reacts with NO–Pt to sustain N_2O production (steps (S8) and (S11)). Thus, at low temperature adsorbed NO is partially reduced by surface hydrogen to form N_2O. This is sustained as long as there is a steady supply of H_2.

These findings also explain why N_2O production exhibits a maximum during NO multi-pulse experiments on Pt/Al_2O_3 in the 250–350 °C temperature range (Fig. 4(c)). At the breakthrough point of NO, the surface is partially covered with N–Pt and NO–Pt, enabling N_2O production. N_2O production is negligible during the first few pulses since the surface is primarily covered with N–Pt and O–Pt species produced from NO decomposition. At intermediate pulse numbers, Pt–O inhibits NO decomposition due to the paucity of vacant sites. This results in an accumulation of NO–Pt which reacts with existing N–Pt adatoms to form N_2O. N_2O is formed only when the surface is nearly devoid of vacant sites. Moreover, since the surface has a limited fraction of vacancies the N_2O cannot readsorb on the Pt. Similarly, N_2O forms during reduction of NO by a limiting supply of H_2 only when the Pt sites are mostly covered with NO–Pt. The pulse of H_2 reacts with NO–Pt, generating N–Pt which can then react with NO–Pt to form N_2O.

Pump-probe experiments carried out under excess NO at 350 °C (Fig. 8) shows the expected trends. The low concentration of H_2 results in the partial reduction of NO on the surface. N_2 formed in the first 50 pulses is produced exclusively from NO decomposition, after which the Pt surface is partially covered with surface oxygen, inhibiting further NO decomposition. This results a partial shift of the selectivity from N_2 to N_2O (step (S4)). NH_3 production is low under such lean conditions due to insufficient H–Pt to react with N–Pt or NO–Pt.

This picture changes in the presence of excess H_2. Experiments carried out at 150 °C (Fig. 7) reveal there are sufficient H adatoms to react with NO–Pt, leading to both N_2 and NH_3 formation. Unreacted H_2 in the outlet indicates that the surface is regenerated under these conditions. NO is not observed in the outlet indicating its complete consumption to NH_3 and N_2. The production of N_2 is far below the stoichiometric level based on the amount of NO fed, but it is comparable to the N_2 produced during NO pulsing experiment at 150 °C (Fig. 4 (a)). One can infer from these results that the N_2 formed under both conditions come primarily from NO decomposition, which is limited by NO bond scission. The remainder of the NO reacts with excess of H_2, forming NH_3, as discussed next.

The pump-probe experiments with excess H_2 reveal an interesting competition between N_2 and NH_3 production. The H_2 serves two roles under these conditions. First, it scavenges O–Pt, freeing sites for NO adsorption. Second, it reacts with NO–Pt, producing both N–Pt and NH–Pt via steps (S11) and (S12), respectively. The production of N_2 results from the scission of the NO bond, be it direct (step (S2)) or by reaction with H–Pt (step (S11)). The reducing environment favors ammonia production (steps (S11)–(S16)) as opposed to N_2O production (steps (S11) and (S4)); hence N_2O is essentially absent in the effluent. Again, the late appearance of both NH_3 and H_2O is due to their slow desorption

from Pt and Al_2O_3. For example, in the monolith temperature ramp experiment (Fig. 14), the adsorption of ammonia and water are evident from the temperature ramp at 600th pulse to 250 °C, when sharp "puffs" of NH_3 and H_2O are observed. At the new temperature level, NH_3 formation decreased compared to 150 °C while N_2 increased. A further ramp in temperature by 100 °C resulted into another NH_3 and H_2O puff, but in a smaller amount than earlier because of reduced adsorption of these species at elevated temperature. At 350 °C, NO decomposition on Pt leads to higher selectivity for N_2 and deposits O adatoms, which are scavenged by hydrogen to form water.

The pump-probe experiments with excess H_2 also show interesting selectivity trends that depend on both temperature and the delay time between the NO and H_2 pulses for both the powder and monolith catalysts. For a fixed delay time of 0.1 s (Fig. 9), the rate of NO decomposition increases with temperature to produce N_2 and surface oxygen; as a result, N_2 production increases from 150 °C to 350 °C. The excess H_2 serves as a scavenger of surface oxygen under these conditions. Ammonia production decreases with increasing temperature even when the H_2 is in excess. In a separate experiment for NH_3 decomposition (not shown here), we did not observe more than 15% of NH_3 decomposing into N_2 and H_2. Thus, the decrease in NH_3 concentration at 350 °C cannot be explained by ammonia decomposition alone and leads us to conclude that ammonia is not even formed under these conditions. Rather, the drop in ammonia production is a result of lack of N–Pt or NO–Pt to react with H_2.

At 350 °C and longer delay times (≥ 1 s) the primary product is N_2 with negligible production of both NH_3 and N_2O. At high enough temperature, the decomposition of NO to N_2 is fast as we observed during the NO decomposition on reduced Pt at 350 °C. A long delay time favors NO decomposition on almost clean Pt surface, forming N and O adatoms. The N adatoms combine to form N_2, while the delayed supply of H_2 simply scavenges the O to form H_2O. There are not enough NO left for H adatoms to react and form NH_3. The pump-probe experiments in excess H_2 at fixed temperature (250 °C) but varied delay time (Fig. 10) isolate the effect of timing of NO and H_2 supply. If the delay time is reduced, there is increased competition between NO decomposition and the NO + H reaction. In the limit of zero delay time (mixed feed), NO + H and N + H occur to form ammonia, overwhelming the decomposition NO to form N_2.

Ammonia formation occurs under conditions of excess H_2 at lower temperature and small delay times (Fig. 11). At low temperature H adatoms remain on the surface while NO–Pt does not decompose readily. These conditions result in the reaction of NO–Pt and H–Pt, forming NH–Pt (S12), which leads to ammonia formation. A mixed feed ($\tau_d = 0$) with excess H_2 similarly leads to excess H–Pt on the surface surrounding NO–Pt or N–Pt species, which leads to ammonia formation. The sensitivity of the product distribution to delay time clearly suggests that the availability of H–Pt to react with NO–Pt is crucial for NH_3 production. The competing pathways are reactions (S11) and (S3), forming N_2, and reactions (S11) and/or (S12) and (S13)–(S16), forming NH_3.

Finally, the results comparing the transport behavior of the powder and monolith catalysts clearly showed an improvement in the response in terms of the elution of the pulsed gas (Fig. 3). The three-zone powder configuration is satisfactory when reaction is fast enough that the reaction is completed within one spacing time. But, for reactions that are slower, such as desorption of products, the three-zone powder configuration causes broader peaks and a creeping baseline. These limitations are minimized in the three-zone monolith configuration. A comparison of the NO pulsing experiments on the powder (Fig. 5) and monolith (Fig. 13) show a reduction in the effluent tail. The three-zone powder configuration shows a slower response for NO because of a lower diffusivity in

the powder phase which is a bottleneck for gas transport. On the other hand, the three-zone monolith configuration does not have such resistance for the gas transport. The slower response also has a contribution from adsorption/desorption of NO on γ-Al$_2$O$_3$ [31–33]. These phenomena lead to an increase in the baseline of NO. A more significant participation of γ-Al$_2$O$_3$ was observed during NO–H$_2$ pump-probe experiments leading to a delay in the NH$_3$ and H$_2$O production. The transient profiles of NH$_3$ and H$_2$O do not show distinguished peaks and have rising baseline effect due to slower desorption from alumina.

5. Conclusions

We have carried out a qualitative study of the NO/H$_2$ on Pt reaction system to elucidate the elementary steps occurring in the reduction of NO in the presence of excess and limiting amount of H$_2$ and to identify the key pathways to products N$_2$, NH$_3$ and N$_2$O. The NO decomposition and reduction pathways are shown to be sensitive not only to temperature and H$_2$/NO feed ratio, but also to the timing of the NO and H$_2$ pulses. The findings underscore the importance of transient effects during NO$_X$ storage and reduction.

The results reveal that the fate of NO on the Pt greatly influences the reduction chemistry. At lower temperature of 150 °C, NO is primarily present in molecular form, occupying multiple Pt sites. Under conditions of a limiting supply of H$_2$ reductant, N$_2$O and N$_2$ are the favored products since there is insufficient hydrogen to react with N adatoms to produce ammonia. Under reducing conditions, the production of ammonia becomes significant even at lower temperature. Since N–O bond scission is slow at this temperature, the formation of ammonia commences with the reduction of molecular NO to N–Pt and NH–Pt with further addition of H leading to ammonia formation. The data indicate that the formation of N$_2$ occurs primarily by a NO decomposition pathway on reduced Pt.

Pump-probe experiments show an interesting effect of delay time between the NO and H$_2$ pulses. For longer delay times, the decomposition of NO proceeds to completion resulting in production of N$_2$ even under overall reducing conditions. The role of H$_2$ is simply to scavenge surface oxygen, cleaning the surface for subsequent NO decomposition. A shorter delay between NO and H$_2$ pulses opens up other options for adsorbed NO, such as the reaction with N to form N$_2$O or the sequential addition of H to form NH$_3$.

The production of N$_2$O shows the sensitive dependence on the concentration of the key surface species. The formation of N$_2$O during reduction of NO in limiting H$_2$ and the noted lack of N$_2$O production during NO pulsing at 150 °C suggests that NO disproportionation is not a favorable path. The presence of both adsorbed NO and adsorbed N species is essential for N$_2$O formation. The absence of N–Pt at 150 °C, because of negligible NO bond scission, results in negligible N$_2$O production during NO pulsing experiments. Similarly, the absence of NO–Pt species at 350 °C for first few pulses contributes to negligible production of N$_2$O.

This study of NO decomposition and reduction chemistry on Pt/Al$_2$O$_3$ provides a framework from which a microkinetic model of NO$_X$ storage and reduction on Pt/BaO/Al$_2$O$_3$ can be developed. NSR is complicated by the existence of spillover processes between the precious metal and storage phases. However, the NO decomposition and reduction pathways studied here remain important ones during the more complex NSR system. This is the focus of ongoing research in our group.

The data reported in this study are not suitable for an unambiguous quantitative analysis, such as to estimate rate constants. The use of the monolith eliminates a key gas transport bottleneck through a layer of powder. The improved signal holds promise for quantitative TAP studies for kinetic parameters estimation and model discrimination. This is an ongoing effort in our laboratory.

References

[1] N. Takahashi, H. Shinjoh, T. Iijima, T. Suzuki, K. Yamazaki, K. Yokota, H. Suzuki, N. Miyoshi, S.i. Matsumoto, T. Tanizawa, T. Tanaka, S.-S. Tateishi, K. Kasahara, Catalysis Today 27 (1996) 63–69.
[2] W. Bogner, M. Kramer, B. Krutzsch, S. Pischinger, D. Voigtlander, G. Wenninger, F. Wirbeleit, M.S. Brogan, R.J. Brisley, D.E. Webster, Applied Catalysis B: Environmental 7 (1995) 153–171.
[3] S.i. Matsumoto, Catalysis Today 29 (1996) 43–45.
[4] M. Shelef, R.W. McCabe, Catalysis Today 62 (2000) 35–50.
[5] R.M. Heck, R.J. Farrauto, Applied Catalysis A: General 221 (2001) 443–457.
[6] T. Miyoshi, S.I. Matsumoto, K. Katoh, T. Tanaka, J. Harada, N. Takahashi, K. Yokota, M. Sugiura, K. Kasahara, Society of Automotive Engineers 950809 (1995) 1361–1370.
[7] K. Papadakis, C.U.I. Odenbrand, J. Sjöblom, D. Creaser, Applied Catalysis B: Environmental 70 (2007) 215–225.
[8] N. Takahashi, K. Yamazaki, H. Sobukawa, H. Shinjoh, Applied Catalysis B: Environmental 70 (2007) 198–204.
[9] W.S. Epling, A. Yezerets, N.W. Currier, Applied Catalysis B: Environmental 74 (2007) 117–129.
[10] J.T. Gleaves, J.R. Ebner, T.C. Kuechler, Catalysis Reviews: Science and Engineering 30 (1988) 49–116.
[11] J.T. Gleaves, G.S. Yablonskii, P. Phanawadee, Y. Schuurman, Applied Catalysis A: General 160 (1997) 55–88.
[12] J. Pérez-Ramírez, E.V. Kondratenko, Catalysis Today 121 (2007) 160–169.
[13] K.S. Kabin, P. Khanna, R.L. Muncrief, V. Medhekar, M.P. Harold, Catalysis Today 114 (2006) 72–85.
[14] V. Medhekar, V. Balakotaiah, M.P. Harold, Catalysis Today 121 (2007) 226–236.
[15] S.O. Shekhtman, G.S. Yablonsky, S. Chen, J.T. Gleaves, Chemical Engineering Science 54 (1999) 4371–4378.
[16] X. Zheng, J.T. Gleaves, G.S. Yablonsky, T. Brownscombe, A. Gaffney, M. Clark, S. Han, Applied Catalysis A: General 341 (2008) 86–92.
[17] Y. Schuurman, Catalysis Today 121 (2007) 187–196.
[18] G.S. Yablonsky, M. Olea, G.B. Marin, Journal of Catalysis 216 (2003) 120–134.
[19] G. Zhou, T. Luo, R.J. Gorte, Applied Catalysis B: Environmental 64 (2006) 88–95.
[20] G.P. Ansell, S.E. Golunski, J.W. Hayes, A.P. Walker, R. Burch, P.J. Millington, Studies in Surface Science and Catalysis 96 (1994) 577–590.
[21] R. Burch, P.J. Millington, A.P. Walker, Applied Catalysis B: Environmental 4 (1994) 65–94.
[22] Z. Jiang, W. Huang, D. Tan, R. Zhai, X. Bao, Surface Science 600 (2006) 4860–4869.
[23] D.C. Ford, Y. Xu, M. Mavrikakis, Surface Science 587 (2005) 159–174.
[24] D.T. Wickham, B.A. Banse, B.E. Koel, Surface Science 223 (1989) 82–100.
[25] N.A. Saliba, Y.L. Tsai, C. Panja, B.E. Koel, Surface Science 419 (1999) 79–88.
[26] J.F. Weaver, J.-J. Chen, A.L. Gerrard, Surface Science 592 (2005) 83–103.
[27] E.S. Putna, J.M. Vohs, R.J. Gorte, Surface Science 391 (1997) L1178–L1182.
[28] S. Shaikhutdinov, M. Heemeier, J. Hoffmann, I. Meusel, B. Richter, M. Bäumer, H. Kuhlenbeck, J. Libuda, H.J. Freund, R. Oldman, S.D. Jackson, C. Konvicka, M. Schmid, P. Varga, Surface Science 501 (2002) 270–281.
[29] W.C. Hecker, A.T. Bell, Journal of Catalysis 92 (1985) 247–259.
[30] M.Y. Smirnov, V.V. Gorodetskii, J.H. Block, Journal of Molecular Catalysis A: Chemical 107 (1996) 359–366.
[31] B. Westerberg, E. Fridell, Journal of Molecular Catalysis A: Chemical 165 (2001) 249–263.
[32] P. Svedberg, E. Jobson, S. Erkfeldt, B. Andersson, M. Larsson, M. Skoglundh, Topics in Catalysis 30/31 (2004) 199–206.
[33] I. Nova, L. Castoldi, L. Lietti, E. Tronconi, P. Forzatti, F. Prinetto, G. Ghiotti, Journal of Catalysis 222 (2004) 377–388.